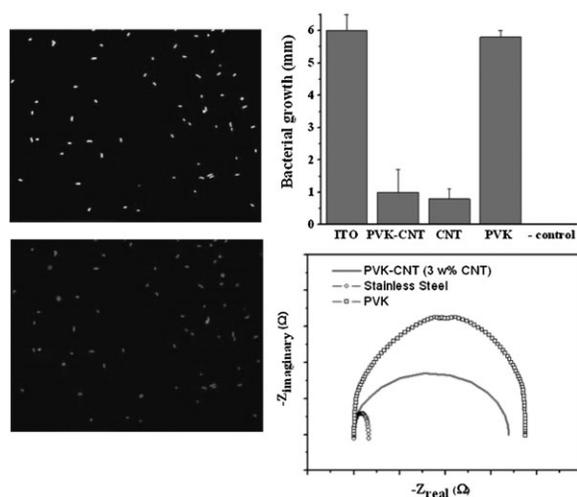# Bactericidal and Anticorrosion Properties in PVK/MWNT Nanocomposite Coatings on Stainless Steel[a]

Catherine M. Santos, Karina Milagros Cui, Farid Ahmed,
Maria Celeste R. Tria, Regina Aileen May V. Vergara,
Al Christopher de Leon, Rigoberto C. Advincula,* Debora F. Rodrigues*

A PVK/MWNT nanocomposite coating on stainless steel is developed and tested for antimicrobial and anticorrosion properties. The coating is prepared via electrochemical deposition onto SS surfaces and is monitored using cyclic voltammetry. High-resolution XPS measurements of the C 1s and N 1s regions are used to estimate the film composition. AFM shows a homogeneous thin film of several μm thickness with well-defined globular domains. The bactericidal functionality of the electrodeposited film is demonstrated by its antibacterial activity against *Escherichia coli*, even with low MWNT loading ($\approx$6%). The excellent anticorrosion property of the coating is demonstrated after 7 d of exposure to NaCl (0.5 M) solution.

Dr. C. M. Santos, F. Ahmed, Prof. D. F. Rodrigues
Department of Civil and Environmental Engineering, University of Houston, Houston, TX 77204-5003, USA
E-mail: dfrigirodrigues@uh.edu
Dr. K. M. Cui, M. C. R. Tria, R. A. M. V. Vergara, A. C. de Leon, Prof. R. C. Advincula
Department of Chemistry and Department of Chemical and Biomolecular Engineering, University of Houston, Houston, TX 772404-5003, USA
E-mail: radvincula@uh.edu

1. Introduction

Bacterial colonization and chemical corrosion are among the major issues commonly encountered on metal surfaces exposed to natural and industrial processes.[1–3] For alloys such as stainless steel (SS) that are used in aquatic environments (e.g., ship hulls, cooling towers, etc.), biofilm formation and corrosion can lead to an increase in energy consumption resulting in higher operational costs.[4] In industries and households (e.g., piping systems, machineries for food processing, etc.), these problems pose serious concerns in terms of safety and long-term application of metallic materials.[5,6] Given that bacterial colonization and

corrosion can be related and in some cases generate complementary problems on various applied metallic surfaces, it is highly desirable to create an effective and robust coating that can address both issues.

The development of polymer nanocomposites as coatings on surfaces has become a fascinating and multidisciplinary area of study, which requires knowledge in material science, nanotechnology, and biology.[7–9] With the large selection of polymers and fillers available to researchers, multifunctional and versatile materials can be easily fabricated. Electroactive polymers have been suggested as effective coating materials to protect against corrosion.[10] Among these polymers, poly(N-vinylcarbazole) (PVK) has been of interest because of its excellent thermal, mechanical, electro-optical properties, and processability.[11–14] PVK can form conjugated polymer network (CPN) films on metal substrates through electrochemical crosslinking of its carbazole moieties.[3,15–17] More importantly, it contains multiple aromatic groups that enable extensive π-π interaction, making it a suitable compatibilizing polymer for carbon-based nanofillers [e.g., carbon nanotubes (CNTs) and graphenes] with known antibacterial properties. Most carbon allotrope nanomaterials are reported to be antibacterial,[18–22] however, CNTs were found to be the most toxic.[23–26]

Although separate reports on the antimicrobial property of CNTs[4,24,25,27] and anticorrosion capability of PVK[3] have been published, to our knowledge, investigations determining the retention of their individual properties when combined as a nanocomposite thin film has not been explored. More recently, it was reported the successful fabrication of well-dispersed PVK/multiwalled carbon nanotube (MWNT) nanocomposites via solution mixing process on different solvents.[28] Herein, we report its direct application as an antibacterial and anticorrosive coating material on metallic substrates. Specifically, we fabricated a thin film of PVK/MWNT coating via electrodeposition to create CPN film of PVK with 6 wt% loading of MWNTs on SS substrates. The bacterial toxicity of the modified films was tested with *Escherichia coli* (*E. coli*), while the anticorrosion property was evaluated by incubating the coated SS substrates in NaCl solution (0.5 M) for 7 d.

2. Experimental Section

2.1. Materials

The MWNTs (purity $\geq$ 95%) used in this study were purchased from Baytubes (C150 P). The MWNTs were produced in a high-yield catalytic process based on chemical vapor deposition (CVD). The outer and inner diameter, length, and density of the MWNTs were 13 nm, 4 nm, 1 μm, and 130–150 kg · m^{-3}, respectively. The MWNTs were further purified by heating at 200 °C for 6 h prior to use. The PVK was purchased from Sigma-Aldrich Chemicals (USA)

($\overline{M}_w \approx$ 25 000–50 000 g · mol^{-1}). All solvents were purchased from Sigma-Aldrich (USA). All solvents were of analytical grade and were used without further purification. SS coupon (Alfa Aesar, USA) was used as the substrates for the PVK/MWNT CPN film fabrication. The SS was cleaned by sequentially sonicating in deionized water, isopropyl alcohol, hexane and toluene, each for 15 min and the substrates were dried in an oven and under a stream of N$_2$. Prior to film deposition, the SS was first plasma cleaned for 3 min.

2.2. Preparation of PVK/MWNT Nanocomposite Solution

The PVK/MWNT (97:3 wt% ratio PVK/MWNT) was prepared according to a previously reported procedure.[28] Briefly, a 97:3% (w/v) ratio of PVK was prepared in methylene dichloride (CH$_2$Cl$_2$) or N-cyclohexyl-2-pyrrolidone (CHP). The purified MWNT (5 mg · mL^{-1}) was first dissolved in CHP and sonicated for 4 h. The PVK was dissolved in CH$_2$Cl$_2$ also by sonication process for 30 min. The PVK solution was then slowly mixed to the MWNT solution and was followed by sonication for 1 h. The PVK/MWNT dispersion was centrifuged (4400 rpm, 1 h) and the black precipitate was removed. The remaining solution of PVK/MWNT dispersion was then treated with methanol (5 mL) and again centrifuged (4400 rpm) for 30 min. The black precipitate was collected and redispersed in CH$_2$Cl$_2$ followed by 20 min of ultrasonication. This procedure furnished a stable PVK/MWNT solution.

2.3. Preparation of PVK/MWNT Nanocomposite Films

The solution for electrodeposition was prepared by mixing 0.1 M tetrabutylammonium hydroxide (TBAH, 2 mL) in acetonitrile with PVK/MWNT (50 μL) at 97:3 wt% ratio as described above. The PVK/MWNT film was deposited onto bare SS (a 300 series 18/10 type) by repeatedly scanning the potential between 0 and 1500 mV at a scan rate of 10 mV · s^{-1} for 50 cycles. Ag and Pt wires were used as the reference and counter electrode, respectively. The deposited film was washed with acetonitrile (3 ×) to remove any unbound material from the surface.

2.4. Characterization of PVK/MWNT Nanocomposite Films

Attenuated total reflectance infrared (ATR-IR) spectra were recorded using an FTS 7000 Digilab Spectrometer within the 700–3500 cm^{-1} range.

X-ray photoelectron spectroscopy (XPS) measurements of the samples were performed using a PHI 5700 spectrometer equipped with a monochromatic Al K$_\alpha$ X-ray source ($h\nu =$ 1486.7 eV) incident at 90° relative to the axis of a hemispherical energy analyzer. The spectrometer was operated both at high and low resolutions with pass energies of 23.5 and 187.85 eV, respectively, a photoelectron take off angle of 45° from the surface, and an analyzer spot diameter of 1.1 mm. High-resolution spectra were obtained for photoelectrons emitted from C 1s and N 1s. All spectra were collected at room temperature with a base pressure of 10^{-8} torr. Electron binding energies were calibrated with respect to the C 1s line at 284.8 eV.

A PHI Multipak software (ver 5.0A) was used for all data processing. The high-resolution data was first analyzed by background subtraction using the Shirley routine and a subsequent nonlinear fitting to mixed Gaussian/Lorentzian functions. Atomic compositions were derived from the high-resolution scans. Peak areas were obtained after subtraction of the integrated baseline and corrected for sensitivity factors.

The electrodeposited PVK/MWNT and PVK morphologies on SS were characterized by AFM. The topography measurement was done under ambient conditions with a PicoSPM II (PicoPlus, Molecular Imaging-Agilent Technologies) in the intermittent contact mode. Images obtained were processed using Gwyddion software (2.13).

2.5. Bacterial Adhesion Measurements

2.5.1. Bacterial Culture

A single isolated *E. coli* K12 MG1655 colony was inoculated in 5 mL tryptic soy broth (TSB) overnight at 35 °C. The bacterial culture was centrifuged at 3000 rpm for 10 min, and the bacteria pellet was resuspended in TSB. The optical density of the suspension was adjusted to 0.5 at 600 nm, which corresponds to a concentration of 10^7 colony forming units per milliliter (CFU · mL^{-1}).

2.5.2. Plate Agar Test

The plate agar test performed on modified SS substrate was based on previously reported protocol.[29] The unmodified SS, electrodeposited PVK/MWNT (97:3 wt% PVK/MWNT), electrodeposited PVK, and spin coated MWNT-modified films on SS were individually placed in a 12 well-plate (Falcon). To each well was added 1.0 mL of bacterial culture and then incubated at 37 °C (without shaking) for 2 h. As a negative control, an unmodified surface incubated in sterile media was used. The film samples were removed and rinsed with PBS to wash any unattached bacteria on the surfaces. The surfaces were then placed onto a tryptic soy agar (TSA) plates (with the coated side down onto the agar surface) and incubated overnight at 35 °C. Photographs from the agar plates were taken with a digital camera and the bacterial growth around each SS coupon plate was measured using a caliper micrometer.

2.6. Antibacterial Measurements on SS Substrates

Electrodeposited PVK/MWNT (97:3 wt% PVK/MWNT), electrodeposited PVK, spin-coated MWNT-modified films, and unmodified SS substrate were individually placed in a 12 well-plate (Falcon). To each well was added 1.0 mL of bacterial culture and then incubated at 37 °C (without shaking) for 2 h. The samples were then removed and immediately prior to viewing were stained with 3 mL of L7007 Life-Dead stain solution for 10 min purchased from Molecular Probes (Leiden, The Netherlands). The solution contains a green fluorescent dye (SYTO 9), which aims to stain total bacterial cells, and a red fluorescence dye (propidium iodide, PI) for detection of dead cells. After the staining, the surfaces were placed on microscope slides, covered with a cover slip and imaged using BX 51 Olympus Fluorescent Microscope equipped with a DP72 digital camera under 40× objective. All images were acquired and analyzed using cell Sens Dimension software (Olympus). Percent loss of viability was calculated as the percent of the ratio of the total number of dead cells to the total number of bacteria attached. All data were expressed as the mean number of bacteria ± standard deviation of two experiments (three replicates at two different times).

2.7. Corrosion Measurement

The unmodified SS, electrochemically crosslinked PVK, and PVK/MWNT CPN films on SS were immersed in 0.5 M NaCl solution for 7 d. Electrochemical impedance spectroscopy (EIS) (Princeton Applied Research Parstat 2263) was used to investigate the change in the electrochemical system and the interface after 7 d of exposure to NaCl solution. The EIS measurements for the films were performed under an open circuit potential with an ac frequency ranging from 100 000 to 0.01 Hz and an excitation signal of 10 mV. All electrochemical experiments were carried out at room temperature.

3. Results and Discussion

3.1. PVK/MWNT Film Fabrication and Characterization

The fabrication of the PVK/MWNT CPN films was performed electrochemically. Figure 1 shows the cyclic voltammetry (CV) plot during the electrodeposition of the PVK/MWNT nanocomposite on an SS surface. The peaks showed the characteristic behavior of PVK, which is the electroactive component of the nanocomposite. The onset of oxidation in the first cycle occurred at about 1.05 V, which is typical in the anodic scans of PVK.[8] The lowering of the onset of oxidation was evident as the cycle increased. This was indicative of the lower oxidation potential for the more extended conjugated species formed after each cycle. However, the reduction peak was not evident (irreversible
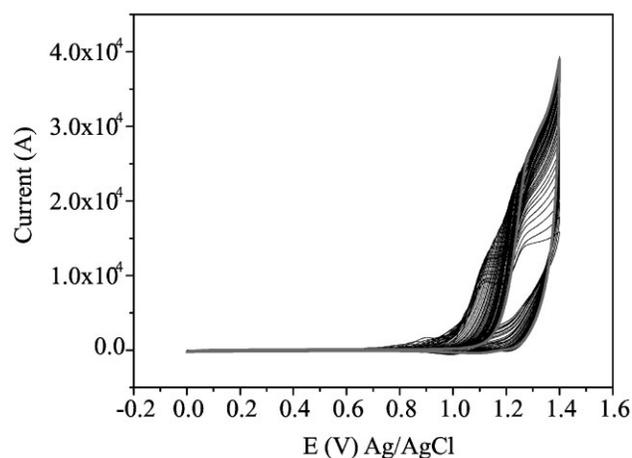

Figure 1. CV plot of the electrodeposition of PVK/MWNT where the gray plot marked the CV data for the first cycle.

Materials
Views
www.MaterialsViews.com

Macromol. Mater. Eng. **2012,** *297,* 807–813
© 2012 WILEY-VCH Verlag GmbH & Co. KGaA, Weinheim
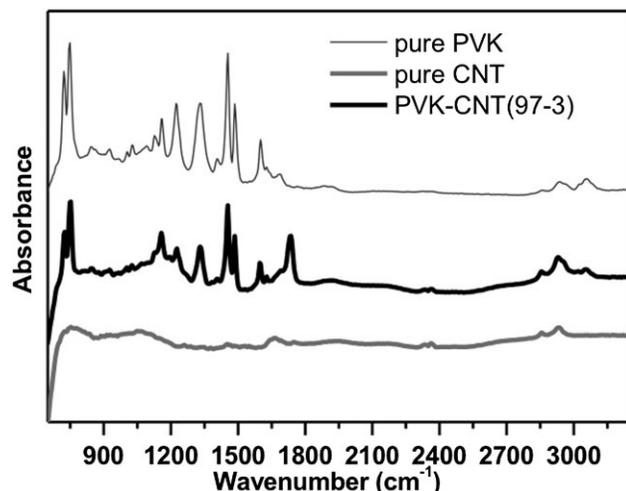
Macromolecular
Journals

809

Figure 2. ATR-IR spectra of pure PVK, PVK/MWNT (97:3 PVK/MWNT wt%) nanocomposite and pure MWNT.

process), which was probably due to the presence of MWNT in the sample that slowed down the charge-transfer process.

The successful electrodeposition of the CPN thin film of PVK/MWNT was confirmed through ATR-IR spectroscopy. The ATR-IR spectrum (Figure 2) of PVK showed the following characteristic peaks: 1626 (C=C stretching vibration), 1459 (ring vibration of *N*-vinylcarbazole), 1326 (>CH_2 deformation), 1220 (C—N stretching of vinyl carbazole), 744 (>CH_2 rocking vibration), and 720 cm^{-1} (ring deformation of substituted aromatic structure). However, for the PVK/MWNT modified film, similar peaks with little variation on the stretching frequencies were observed when compared to the control containing PVK only. In particular, peak shifts toward higher wavenumber were observed from 744 to 749, from 1459 to 1449, and from 1626 to 1620 cm^{-1}.[30] The shift in peaks can be attributed to the increase in conjugation length of PVK and the effective wrapping of the MWNT by PVK upon electrodeposition.[28]

XPS measurements were performed to account for the elemental composition of the films (PVK/MWNT, MWNT, and PVK). The high resolution scans of the C 1s and N 1s regions (Figure 3a and b) obtained by XPS were used to calculate C/N ratios of the PVK/MWNT and pure PVK films, which were 9.8 and 9.2, respectively. The slightly higher C/N ratio observed for PVK/MWNT film was caused by the incorporation of the carbon-containing MWNT nanofiller. From the C/N ratios for the PVK and PVK/MWNT films, the amounts of PVK and MWNT in the nanocomposite thin films were estimated to be 94 and 6%, respectively. These values were close to initial loading concentrations of PVK (97 wt%) and MWNT (3 wt%) in solutions prior to the electrodeposition.
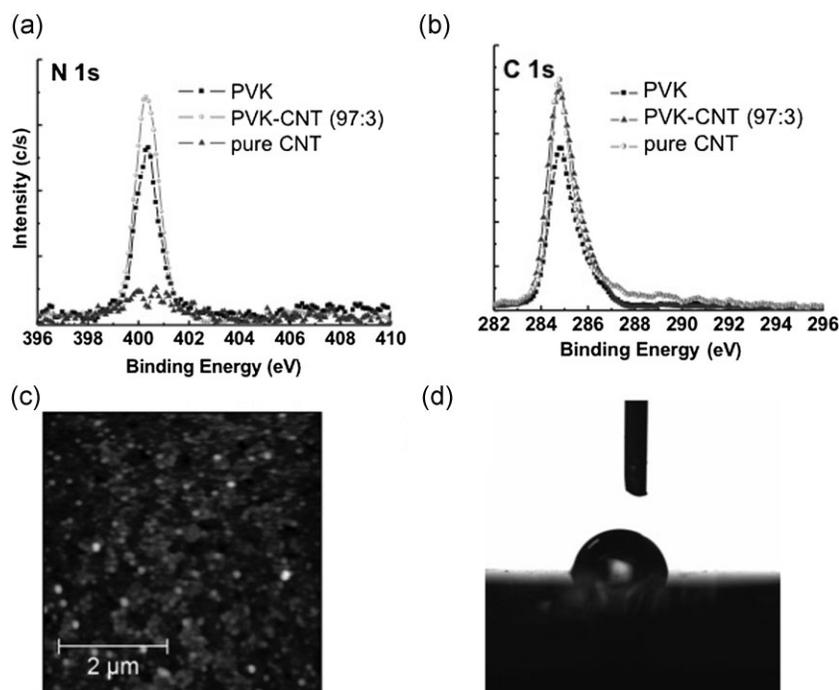
The surface morphology of electrodeposited PVK/MWNT and PVK surfaces were investigated using atomic force microscopy (AFM). The topography of both the nanocomposite and the PVK CPN-modified surfaces showed well-defined globular domains and excellent surface coverage (Figure 3c). Globular structures are typically observed on surfaces coated with PVK.[15] However, the PVK/MWNT film showed a rougher surface than the PVK film alone, with an average surface roughness of 8.4 and 2.9 nm, respectively (Figure S1b of Supporting Information). The change in surface roughness can be correlated with the higher water contact angle (WCA) observed for the resulting PVK/MWNT film (89.1°) and is indicative of its lower surface energy due to the presence of more hydrophobic MWNTs as compared to the pure PVK surface, which has a WCA of 53.3°.

Figure 3. Surface characterization of the PVK/MWNT coated film: XPS narrow scan spectra (a) N 1s and (b) C 1s of the MWNT, PVK, and PVK/MWNT modified SS surface. (c) AFM image ($3 \times 3 \mu m^2$) of electrodeposited PVK/MWNT on SS substrate. (d) Static WCA of the PVK/MWNT surface (See Figure S2 in the Supporting Information for color images).

3.2. Antibacterial Measurements

To evaluate the antibacterial activity of the nanocomposite (PVK/MWNT)
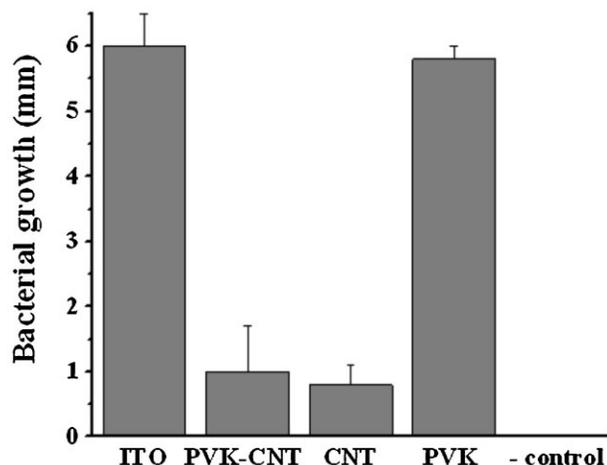
www.MaterialsViews.com

Figure 4. Toxicity of PVK/MWNT CPN films against *E. coli*. (a) Growth measurements of bacterial cells attached to the surfaces. The cells were grown on agar plates.

Figure 5. (a) Correlation of % nonviable bacteria (% loss of viability) attached on each surface, (b) fluorescence images of *E. coli* on MWNT-modified, PVK/MWNT-modified, and unmodified SS films. Images were obtained with 40× objective using fluorescein isothiocyanate (FITC) and tetramethyl rhodamine iso-thiocyanate (TRITC) filters for green fluorescence produced by SYTO 9, and for red fluorescence produced by PI, respectively. The total bacteria are stained with SYTO 9 and are presented on the left column. While the membrane compromised bacteria stained with PI are presented on the right column (see Figure S3 in the Supporting Information for color images).

modified coatings, live bacteria proliferation were determined by plate agar method. Results showed that bacterial growth was reduced on MWNT modified coatings (i.e., MWNT and PVK/MWNT) as compared to the unmodified coatings (Figure 4). The PVK/MWNT and MWNT modified substrates inhibited bacterial growth by up to 83 and 87%, respectively. The PVK modified surface alone however did not show any bacterial inhibition.

Cell viability measurements were obtained through the live and dead fluorescence staining technique with SYTO 9 and PI. SYTO 9 stains viable cells, while bacteria with compromised membranes (dead cells) are stained by PI. The percentage of dead bacteria (% loss of viability) was expressed as the ratio of the number of cells stained with PI divided by the total number of bacteria. Figure 5a presents fluorescence-based viability results for cells attached to PVK/MWNT modified surfaces. Clearly the MWNT and PVK/MWNT films showed greater toxicity than the PVK alone and the unmodified substrate (Figure 5a). MWNT and PVK/MWNT showed 95 and 90% of dead cells, respectively. This antibacterial property is consistent with the literature on MWNT-based materials,[22,24,26] where the possible mechanisms of toxicity are caused by oxidative stress and membrane damage.[24]

It is worth noting that the antibacterial property of the nanocomposite coating is comparable to pure MWNT coated surfaces, even though the nanocomposite surfaces contained only ≈6% of MWNT, based on the XPS results. This is probably due to the high and effective dispersibility of MWNT within the nanocomposite matrix prior to electrodeposition, which led to a homogeneous coverage of the surface. The homogeneous coating probably led to a better exposure of the MWNTs to the bacteria causing higher antimicrobial effects.
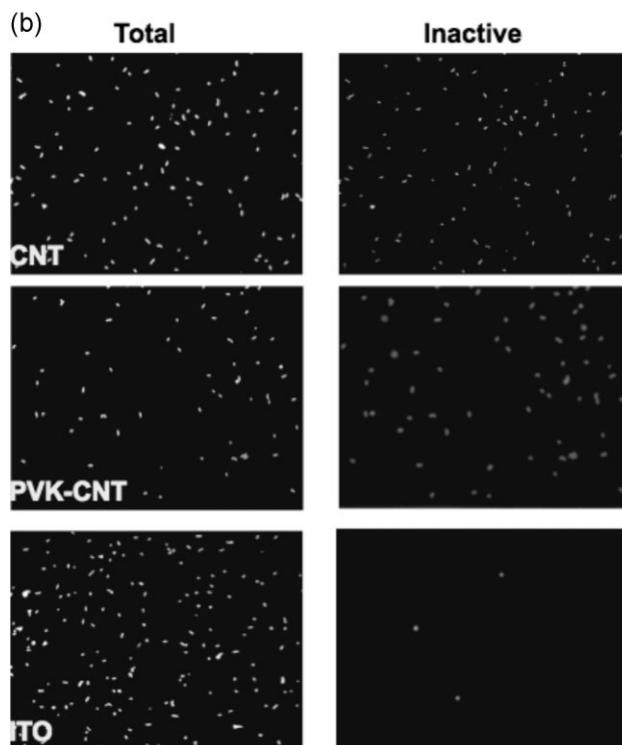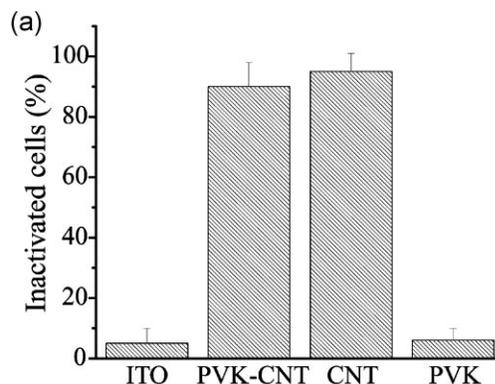
3.3. EIS Measurements

EIS was employed to evaluate the corrosion behavior of the PVK–CPN coated films (PVK and PVK/MWNT) on SS coupons. EIS is considered to be a powerful tool in probing charge transfer phenomena and interfacial ion transfer on films.[31,32] The corrosion resistance of the bare SS, PVK
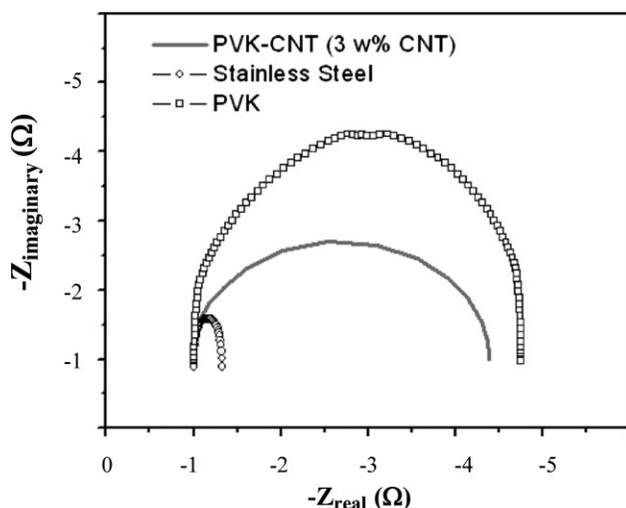
Figure 6. Nyquist plot of electrodeposited PVK/MWNT (97:3 wt% PVK/MWNT), SS, and electrodeposited PVK after 7 d exposure in 0.5 M NaCl solution.

coated SS, and PVK/MWNT-modified SS were analyzed after immersion of the films in 0.5 M NaCl for 7 d. All samples show capacitive behavior as presented in the semi-circle plot (Figure 6).

The behavior of the samples in corrosive environment can be better understood by comparing the relative magnitude of their polarization resistance. Polarization resistance quantifies the ability of the system to resist the transfer of charge during the reduction/oxidation reaction: a large polarization resistance indicates a slow charge-transfer step. Relative magnitude of the polarization resistance can be determined by subtracting the real-axis value at the high frequency intercept (near the origin) from the real-axis value at the low frequency intercept (farther from the origin). Polarization resistance is therefore related to the diameter of the semi-circle–larger diameter corresponds to larger polarization resistance. Generally, high polarization resistance was observed for the PVK containing surfaces (i.e., PVK and PVK/MWNT films). The highest polarization resistance was observed for the PVK film alone followed by the PVK/MWNT coated surface. As expected, the unmodified SS coupon had the smallest diameter and therefore the lowest polarization resistance. In some cases, scattered Nyquist plots were observed for the SS coupons (results not shown). This can be interpreted as the beginning of the corrosion process,[33] possibly due to the breakdown of the passive layer on the surface upon exposure to chloride ions (Cl$^-$). Chloride ion has been reported as an aggressive ion, which can penetrate the surface and facilitate the corrosion process.[34] The results suggest that the CPN films containing PVK provides an effective anticorrosion coating that prevents Cl$^-$ to diffuse through the passive layer. The presence of a

conducting material such as MWNTs can, however, lower the polarization resistance observed. In addition, films fabricated with the nanocomposites were observed to be rougher (as shown by the higher calculated rms) than the electrodeposited PVK. Visualization showed slightly more brownish color of the PVK/MWNT film on SS compared to the PVK film which has a lighter brownish tint (picture is unreported).

4. Conclusion

In conclusion, we demonstrated that the electrodeposited PVK/MWNT nanocomposite films can have simultaneous bactericidal and anticorrosion properties. The PVK/MWNT surfaces showed enhanced toxicity against *E. coli* as compared to the uncoated and PVK modified SS substrates. Corrosion inhibition was also demonstrated by the nanocomposite coated SS coupons, even after 7 d of exposure to 0.5 M NaCl solution. The results suggested that the antimicrobial and anticorrosion behavior of the electrodeposited PVK/MWNT nanocomposite thin films can be attributed to the combined and known properties of each component. This bi/functional nanocomposite film has potential application for coating materials exposed to physiological (biomedical) and marine (industrial) environments where both biofilm formation and corrosion are of major concern.

[1] G. Wang, H. Zreiqat, *Materials* **2010**, *3*, 3994.
[2] K. A. Natarajan, *Corros. Sci. Technol.* **2009**, 95.
[3] A. F. Frau, R. B. Pernites, R. C. Advincula, *Indus. Eng. Chem. Res.* **2010**, *49*, 9789.
[4] V. K. K. Upadhyayula, V. Gadhamshetty, *Biotechnol. Adv.* **2010**, *28*, 802.
[5] W. M. Dunne, Jr., *Clin. Microbiol. Rev.* **2002**, *15*, 155.
[6] T. Mattila-Sandholm, G. Wirtanen, *Food Rev. Int.* **1992**, *8*, 573.
[7] L. Zhang, *Adv. Mater. Res.* **2011**, *139–141*, 1.
[8] R. Verdejo, M. M. Bernal, L. J. Romasanta, M. A. Lopez-Manchado, *J. Mater. Chem.* **2011**, *21*, 3301.
[9] S. Kanagaraj, *Mater. Sci. Found.* **2010**, *65–66*, 255.
[10] J. M. Yeh, K. C. Chang, *J. Ind. Eng. Chem.* **2008**, *14*, 275.

[11] J. A. Ouintana, J. M. Villalvilla, P. Boj, M. A. Diaz-Garcia, *Mol. Org. Electron. Dev.* **2010**, 233.

[12] P.-L. T. Boudreault, S. Beaupre, M. Leclerc, *Polym. Chem.* **2010**, *1*, 127.

[13] J. Davenas, A. Ltaief, V. Barlier, G. Boiteux, A. Bouazizi, *Mater. Sci. Eng., C: Biomim. Supramol. Syst.* **2008**, *28*, 744.

[14] Y. Z. Wang, A. J. Epstein, *Acc. Chem. Res.* **1999**, *32*, 217.

[15] T. M. Fulghum, P. Taranekar, R. C. Advincula, *Macromolecules* **2008**, *41*, 5681.

[16] P. Taranekar, T. Fulghum, D. Patton, R. Ponnapati, G. Clyde, R. Advincula, *J. Am. Chem. Soc.* **2007**, *129*, 12537.

[17] A. Baba, K. Onishi, W. Knoll, R. C. Advincula, *J. Phys. Chem. B* **2004**, *108*, 18949.

[18] C. M. Santos, M. C. Tria, R. A. M. V. Vergara, F. Ahmed, R. Advincula, D. F. Rodrigues, *Chem. Commun.* **2011**, *47*, 8892.

[19] O. Akhavan, E. Ghaderi, *ACS Nano* **2010**, *4*, 5731.

[20] W. Hu, C. Peng, W. Luo, M. Lv, X. Li, D. Li, Q. Huang, C. Fan, *ACS Nano* **2010**, *4*, 4317.

[21] D. Y. Lyon, P. J. J. Alvarez, *Environ. Sci. Technol.* **2008**, *42*, 8127.

[22] D. F. Rodrigues, M. Elimelech, *Environ. Sci. Technol.* **2010**, *44*, 4583.

[23] L. R. Arias, L. Yang, *Langmuir* **2009**, *25*, 3003.

[24] S. Kang, M. Herzberg, D. F. Rodrigues, M. Elimelech, *Langmuir* **2008**, *24*, 6409.

[25] S. Kang, M. Pinault, L. D. Pfefferle, M. Elimelech, *Langmuir* **2007**, *23*, 8670.

[26] S. Liu, L. Wei, L. Hao, N. Fang, M.-W. Chang, R. Xu, Y. Yang, Y. Chen, *ACS Nano* **2009**, *3*, 3891.

[27] P. Lu, Y.-L. Hsieh, *ACS Appl. Mater. Interfaces* **2010**, *2*, 2413.

[28] K. M. Cui, M. C. Tria, R. B. Pernites, C. A. Binag, R. C. Advincula, *ACS Appl. Mater. Interfaces* **2011**, *3*, 2300.

[29] R. Muller, A. Eidt, K. A. Hiller, V. Katzur, M. Subat, H. Schweikl, S. Imazato, S. Ruhl, G. Schmalz, *Biomaterials* **2009**, *30*, 4921.

[30] S. P. Li, Y. J. Qin, J. H. Shi, Z. X. Guo, L. Yongfang, D. B. Zhu, *Chem. Mater.* **2005**, *17*, 130.

[31] F. Mansfeld, ''Inhibitors and Coatings'', in: *Electrochemical and Optical Techniques for the Study and Monitoring of Metallic Corrosion* (Eds: M. G. S. Ferreira, C. A. Melendres), Vol. 203, NATO ASI Series E, Kluwer, Dordrecht **1991**, p. 521.

[32] F. Mansfeld, *Mater. Corros.* **2003**, *54*, 489.

[33] V. Palanivel, Y. Huang, W. J. Ooij, *Prog. Org. Coat.* **2005**, *53*, 153.

[34] K. Aramaki, T. Shimura, *Corros. Sci.* **2010**, *52*, 1464.